International Journal of Biological Macromolecules 233 (2023) 123395

Contents lists available at ScienceDirect

International Journal of Biological Macromolecules

journal homepage: www.elsevier.com/locate/ijbiomac

Post grafted gallic acid to chitosan-Ag hybrid nanoparticles via free radical-induced grafting reactions

Mohamed A. Mohamady Hussein [a,i,*], José Manuel Olmos [b], Michał K. Pierański [c], Mariusz Grinholc [c], Eva Miriam Buhl [d], Oguzhan Gunduz [e], Ahmed M. Youssef [f], Carlos M. Pereira [g], Ibrahim M. El-Sherbiny [h,**], Mosaad Megahed [a]

[a] Clinic of Dermatology, RWTH Aachen University Hospital, Aachen 52074, Germany
[b] Departamento de Química Física Aplicada, Facultad de Ciencias, Universidad Autónoma de Madrid, 28049 Madrid, Spain
[c] Laboratory of Photobiology & Molecular Diagnostics, Intercollegiate Faculty of Biotechnology, University of Gdansk & Medical University of Gdansk, Gdansk, Poland
[d] Electron Microscopy Facility, Institute of Pathology, RWTH Aachen University Hospital, 52074 Aachen, Germany
[e] Center for Nanotechnology & Biomaterials Application and Research (NBUAM), Marmara University, Istanbul 34722, Turkey
[f] Packaging Materials Department, National Research Centre, 33 El Bohouth St. (Former El Tahrir St.), Dokki, Giza, P.O. 12622, Egypt
[g] Centro de Investigação em Química da Universidade do Porto, Departamento de Química e Bioquímica, Faculdade de Ciências da Universidade do Porto, Porto, Portugal
[h] Nanomedicine Laboratories, Center for Materials Science (CMS), Zewail City of Science and Technology, 6th of October, Giza 12578, Egypt
[i] Department of Pharmacology, Medical Research Institute, National Research Centre, 33 El Bohouth St., Dokki, Giza 12622, Egypt

ARTICLE INFO

Keywords:
Chitosan–Ag nanoparticles
Gallic acid
Antibacterial and antioxidant activity

ABSTRACT

The present study proposes two unique systems using free radical-induced grafting reactions to combine Ag, chitosan (CS) and gallic acid (GA) into a single particulate nanostructure. GA-grafted-CS (GA-g-CS) was used to reduce Ag^{+} to Ag^{0}, and producing Ag-GA-g-CSNPs (hybrid NPs I). Also, GA was grafted into CS–AgNPs, to form GA-g-CS AgNPs (hybrid NPs II). Although there were previous attempts to graft GA into CS, this is first time to graft GA into CS–AgNPs. The study aimed to enhance biocompatibility, antibacterial and antioxidant properties of CS–AgNPs via grafted GA. Grafting GA into CS–AgNPs was confirmed by UV–Vis, DLS, DSC/TGA, XRD, EDX and FTIR. The morphology and size of NPs were studied by TEM and SEM. The decrease of ζ-potential from +50 mV in CS-Ag NPs to +33 and + 29 mV, in the presented 2 nanoforms hybrid NPs I and II, respectively, is an indication for the successful GA graft. Among all samples, hybrid NPs II showed lower toxicity, higher antioxidant and antibacterial activity. The obtained results revealed that grafting GA to CS–AgNPs, as a new method to combine Ag, CS and GA in a uniparticulate structure, is a unique process which may deserve a more future consideration.

1. Introduction

As a result of natural biological processes, reactive oxygen species (ROS). They are also produced through the cellular response to xenobiotics, cytokines, and bacterial invasion [1]. It is highly important to maintain the balance between the produced free radicals and available antioxidants in the human body to avoid any potential harms [2]. Since their wide use in medical and pharmaceutical applications, the metal nanoparticles (NPs) could cause an increase in the produced ROS to non-desired level. There is a tremendous increase in the applications of AgNPs in tissue regeneration owing to their antimicrobial properties. However, AgNPs can cause damages to membrane proteins and DNA associated with emerging many diseases. Such disintegrative effect, caused mainly as a result of ROS produced when applying high doses of AgNPs, reduces drastically the safety of Ag containing polymers (i.e. chitosan, CS) [3–5]. Therefore, there is an important interest in recent years to include antioxidant agents to maintain such balance and to scavenge the excessively produced ROS. One of the well-known

* Correspondence to: M.A.M. Hussein, University Hospital of Aachen, Aachen 52074, Germany.
** Corresponding author.
E-mail addresses: almohammadeymr2023@gmail.com (M.A. Mohamady Hussein), jose.olmos@uam.es (J.M. Olmos), michal.pieranski@phdstud.ug.edu.pl (M.K. Pierański), mariusz.grinholc@biotech.ug.edu.pl (M. Grinholc), ebuhl@ukaachen.de (E.M. Buhl), oguzhan@marmara.edu.tr (O. Gunduz), drahmadyoussef1977@gmail.com (A.M. Youssef), cmpereir@fc.up.pt (C.M. Pereira), ielsherbiny@zewailcity.edu.eg (I.M. El-Sherbiny), mmegahed@ukaachen.de (M. Megahed).

https://doi.org/10.1016/j.ijbiomac.2023.123395
Received 22 November 2022; Received in revised form 6 January 2023; Accepted 19 January 2023
Available online 23 January 2023

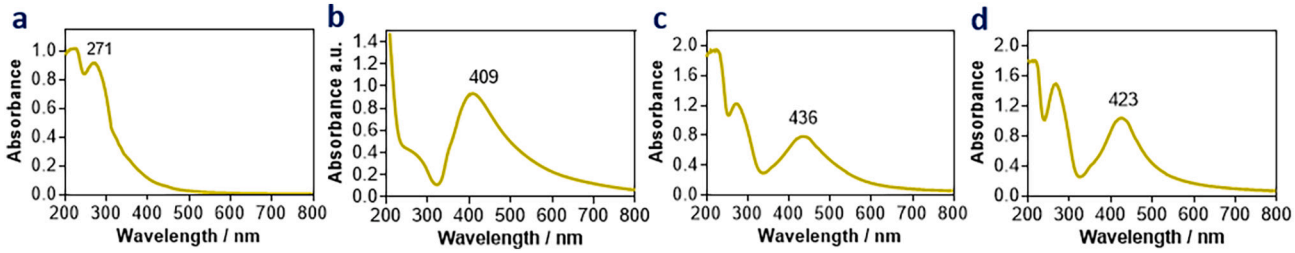

Fig. 1. UV–vis spectroscopy of GA-g-CS (a); CS–AgNPs (b); hybrid NPs I (c); and hybrid NPs II (d).

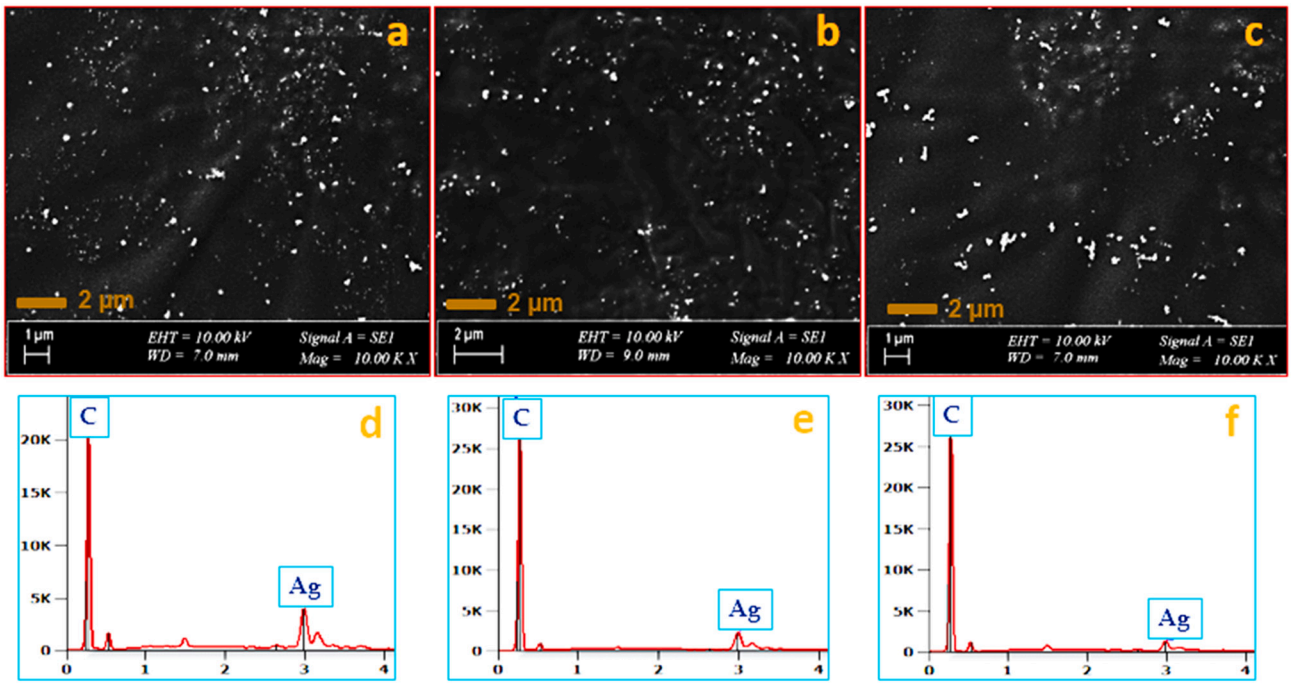

Fig. 2. SEM micrographs of CS–AgNPs (a), hybrid NPs I (b) and hybrid NPs II (c). EDX of CS–AgNPs (d), hybrid NPs I (e) and jhybrid NPs II (f).

antioxidant agents is gallic acid (GA). GA (3,4,5-trihydroxy benzoic acid) is a natural triphenolic compound extracted and purified from different plants such as green tea [6]. The ability of GA to inhibit lipid peroxidation, render it and its derivatives to be widely used in cosmetic, pharmaceutical and food industries [7,8]. Despite the power of GA as antioxidant, GA–free base is rapidly eliminated, poorly absorbed and has a low bioavailability [9,10]. As a consequence, it is not widely used clinically or in food formulations. Nano-formulation is likely to be a promising approach to improve and refine such drawbacks, through conjugation or drug delivery carriers. Functionalized noble metal nanoparticles with GA have proved to present superior antioxidant activity compared to non-functionalized ones [11]. In another approach to maximize the efficiency of GA in pharmaceutical applications, its conjugation with polymers such as CS, alginate [12], PVA and chitooligosaccharides [13] has been tested. CS, a linear polysaccharide of β-(1–4)-linked D-glucosamine and *N*-acetyl-D-glucosamine, is the main derivative of chitin, a natural structural polysaccharide extracted from fungal cell walls, exoskeletons of arthropods, and endoskeletons of cephalopods [14]. The characteristics of CS as low toxic, biocompatible, biodegradable and low immunogenic material make it highly applicable in various biomedical applications, such as antibacterial, tissue engineering and cancer therapy [15–18].

In the study reported by Lunkov et al., they used carbodiimide for conjugation of CS and GA, followed by using the product for producing the AgNPs. However, it was found that the produced NPs were with low zeta potential (ζ-potential) of +8 mV [19]. In particular, the pH at which the processed reaction was 7.5 which considered non-desirable for CS and CS NPs in the aspects of their solubility and cationic ζ-potential where they are likely to aggregate and with a loss in their antibacterial efficiency [20,21]. In addition, this system (carbodiimide-based coupling) employs chemical coupling reagents which are considered as harmful for mammalian cells. It was reported that using this system which requires a large amount of chemical crosslinking agent such as EDC, NHS or DCC, is an expensive and non-ecofriendly in particular when the grafted product is included in food and pharmaceutical industries [22]. Meanwhile, the free radical grafting via applying ascorbic acid (Vc)/hydrogen peroxide (H_2O_2) redox pair as an initiator system, was reported for its much less toxicity than carbodiimide-based coupling [23]. Free radical grafting reaction is cheaper and easily processed even at room temperature to avoid the oxidation and degradation of phenolics. Therefore, using the free radical-mediated reaction via Vc/H_2O_2 redox pair in the current study, would be more economical and ecofriendly than the previously-reported carbodiimide-based chemical coupling method. Rather than, using the synthesized CS-g-GA as a capping agent for Ag atom as reported by Lunkov et al., the current study focuses on the post conjugation of GA to the pre-prepared CS–AgNPs.

Herein, we propose the conjugation of an antioxidant molecule with ROS scavenging property, such as GA, to CS–AgNPs in order to minimize the drawbacks produced by AgNPs efficiently. It is expected that the simultaneous presence of the three agents GA/CS/Ag as a single

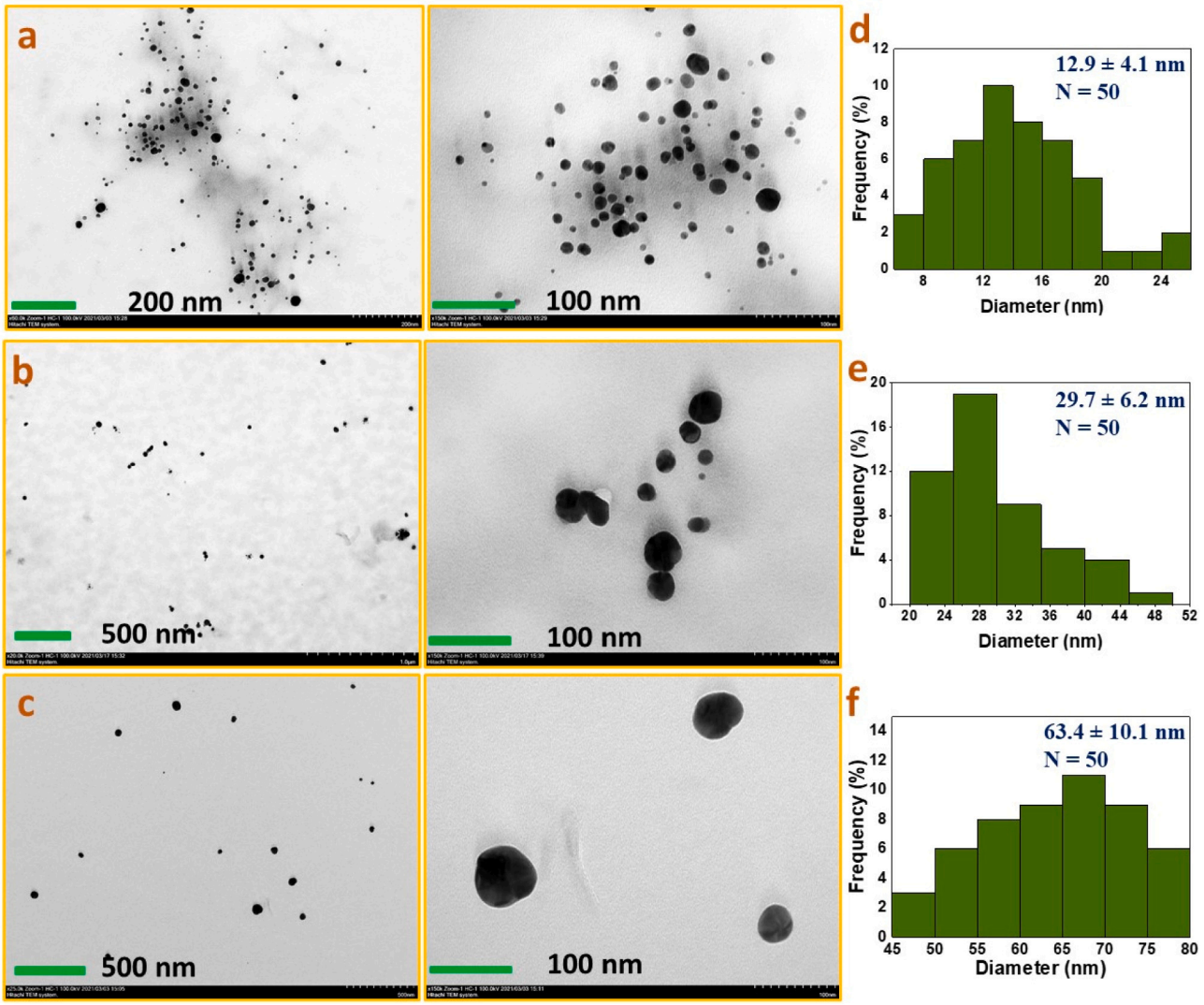

Fig. 3. TEM images (a–c) and particle size distribution histograms (d–f) of the developed CS–AgNPs, hybrid NPs II, and hybrid NPs I, respectively.

nanostructure may provide synergistic action as potent antimicrobial agent. Although CS-AgNPs [24], GA-g-CS [25,26], GA-AgNPs [27] and GA-CSNPs [28] have been previously studied, for the best of our knowledge, it is the first study to employ CS–AgNPs as substrates to conjugate GA via ecofriendly free radical-mediated reaction. It is hypothesized that this system (free radical-mediated reaction, Vc/H_2O_2 redox pair) which employs metallic-based CS-NPs instead of CS as substrates will induce the initiator system to graft GA, hydroxylcinnamic acid (e.g. ferulic acid) or curcumin, more efficiently. Bringing GA/CS/Ag in a single nanostructure, using an ecofriendly reaction system is supposed to be excellent cyto-biocompatible CA-CS-Ag nanocomposites with augmented antibacterial and antioxidant properties. For such purpose, two approaches were employed to prepare GA/CS/Ag nanostructures. First approach used the prepared GA-g-CS as reducing agents for Ag^+ ($Ag NO_3$) and form Ag-GA-g-CSNPs (named hybrid NPs I). Meanwhile, the second one grafted the GA to the pre-prepared CS-AgNPs to form GA-g-CS-AgNPs (named hybrid NPs II). The study compares the two prepared hybrids systems in terms of physicochemical characterizations and biological evaluation.

2. Materials and methods

2.1. Materials

Chitosan (CS) (Mw 60–120 kDa and 82 % of degree of deacetylation), gallic acid ($C_7H_6O_5$), hydrogen peroxide, ascorbic acid and potassium persulphate were purchased from Sigma-Aldrich. Silver nitrate, glacial acetic acid and ABTS (2,2′-azinobis-(3 ethylbenzothiazoline-6-sulfonic acid) solution were acquired from Merck.

2.2. Synthesis of GA/CS/Ag hybrid NPs

The synthesis of GA-g-CS was performed as previously reported [29]. Briefly, chitosan solution (0.5 g) was prepared in 10 mL acetic acid (2 % *v*/v). After that, 1 mL of H_2O_2 (1 mol/mL) containing 0.054 g ascorbic acid was added and kept for 30 min. Then, 0.17:1.0 GA/CS of GA was added to the solution and left overnight. The obtained solution (GA-g-CS) was exposed for dialysis using dialysis tubes, and was then used to reduce Ag salt to form Ag-GA-g-CSNPs (hybrid NPs I). To produce GA grafted to CS–AgNPs, the CS–AgNPs were synthesized by adding a predetermined amount of silver precursor $AgNO_3$ to CS solution to obtain a final concentration of 0.001 mol/L. Followed by adding $NaBH_4$ solution (0.02 mol/L) as a reducing agent dropwise under stirring to give a black brown colloid as an indication for the formation of AgNPs [30,31]. The

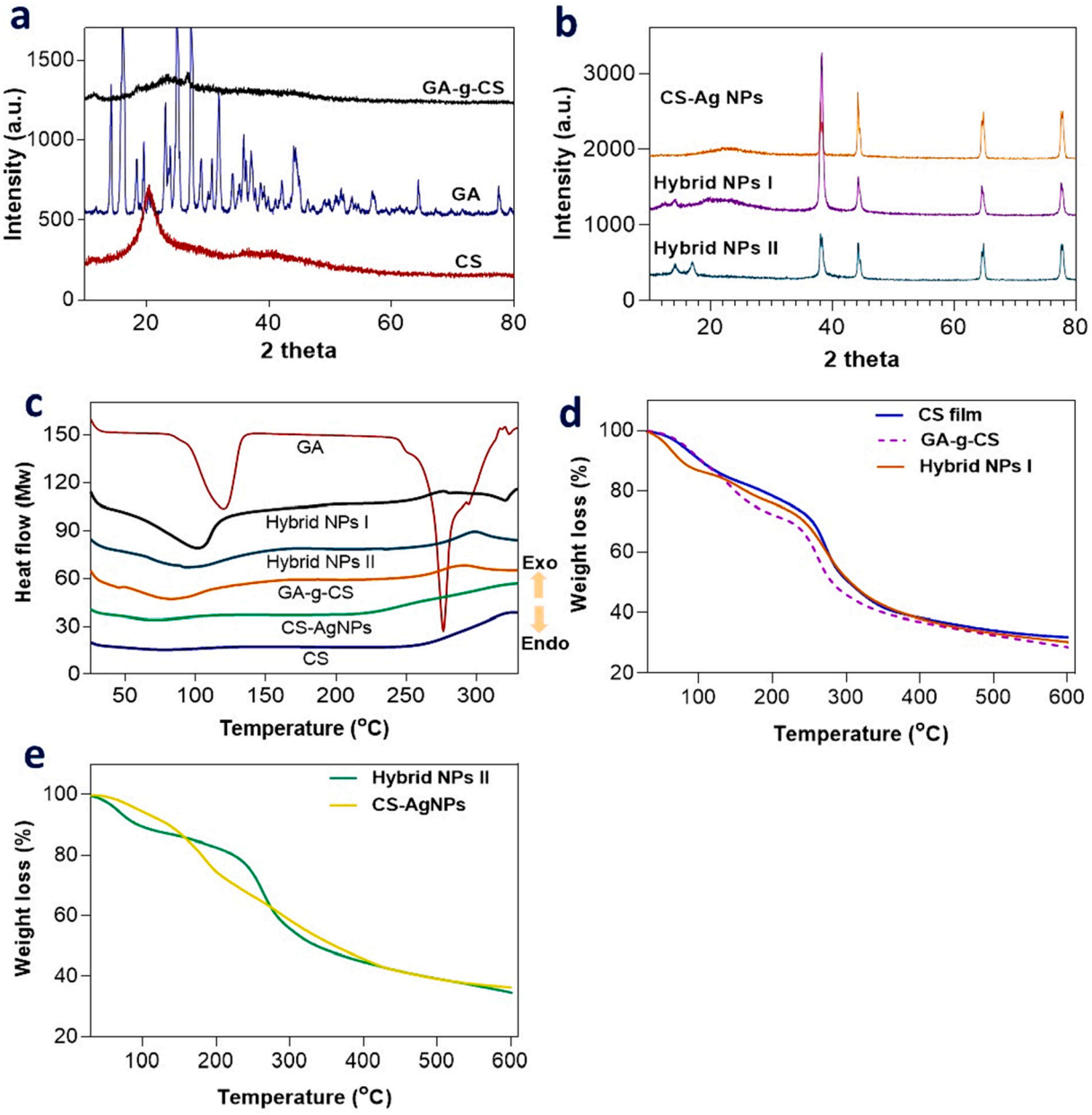

Fig. 4. XRD spectra (a,b); DSC (c); and TGA analysis (d,e) of developed hybrid NPs.

solution was left for a while under stirring until there were no bubbles. The obtained NPs were used to form GA-g-CS AgNPs (hybrid NPs II) in the same steps as stated above. Obtained NPs were then ultra-sonicated (Qsonica Llc, Newtown, CT, USA) for 5 min, 30s pulse on/30s pulse off time with amplitude 70 % in ice-bath to maintain at room temperature.

2.3. Physicochemical characterizations of the hybrid NPs

UV–Vis spectroscopy was used to record the electronic absorption spectra of the developed hybrid NPs by using a T92+ double-beam ultraviolet-visible (UV–Vis) spectrophotometer (PG Instruments, UK) in the range of 300–800 nm. Dynamic light scattering (DLS) was carried out to record both the particle size and the surface zeta potential (ζ potential) using a Malvern Zetasizer Nano ZS (Malvern Instruments Ltd., UK). Particle sizes were evaluated by considering a spherical shape. The chemical composition and the confirmation of the grafted GA to the hybrid NPs was analyzed by Fourier transform infrared (FTIR, FT-IR JASCO 4700, USA) spectroscopy in the range of 4000–400 cm^{-1}. The purity and crystallinity of the developed hybrid NPs were characterized by X-ray diffraction (XRD) analysis using Philips PW 1390 X–ray diffractometer ($\lambda = 1.54056$ Å, 40 kV). The 2θ angle was recorded in the range of 10–80° with a scanning speed of 2°/min. The crystallinity of the developed samples was also calculated using Material Studio Vision (MSV) software, version 4.4. The morphology and shape of the hybrid NPS were imaged with the aid of transmission electron microscopy (Hitachi HT7800) at an accelerating voltage of 100 kV. The samples for TEM images were prepared by depositing 10 μL of the colloidal suspensions on a glow-discharged 200 mesh formvar/carbon film–coated Cu grid. After incubation for 5 min excessive solution was removed with a filter paper and the grid and left for airdrying. ImageJ® was used to generate the histograms of the hybrid NPs size distribution. SEM analysis element analyses was performed on air–dried, platinum–coated samples using scanning electron microscope (Philips/FEI XL 30 SEM) and operated at accelerating voltage of 25 kV. Scanning electron microscope integrated with energy-dispersive X-ray spectroscopy (SEM-EDX) were employed to characterize and confirm the biosynthesis of the

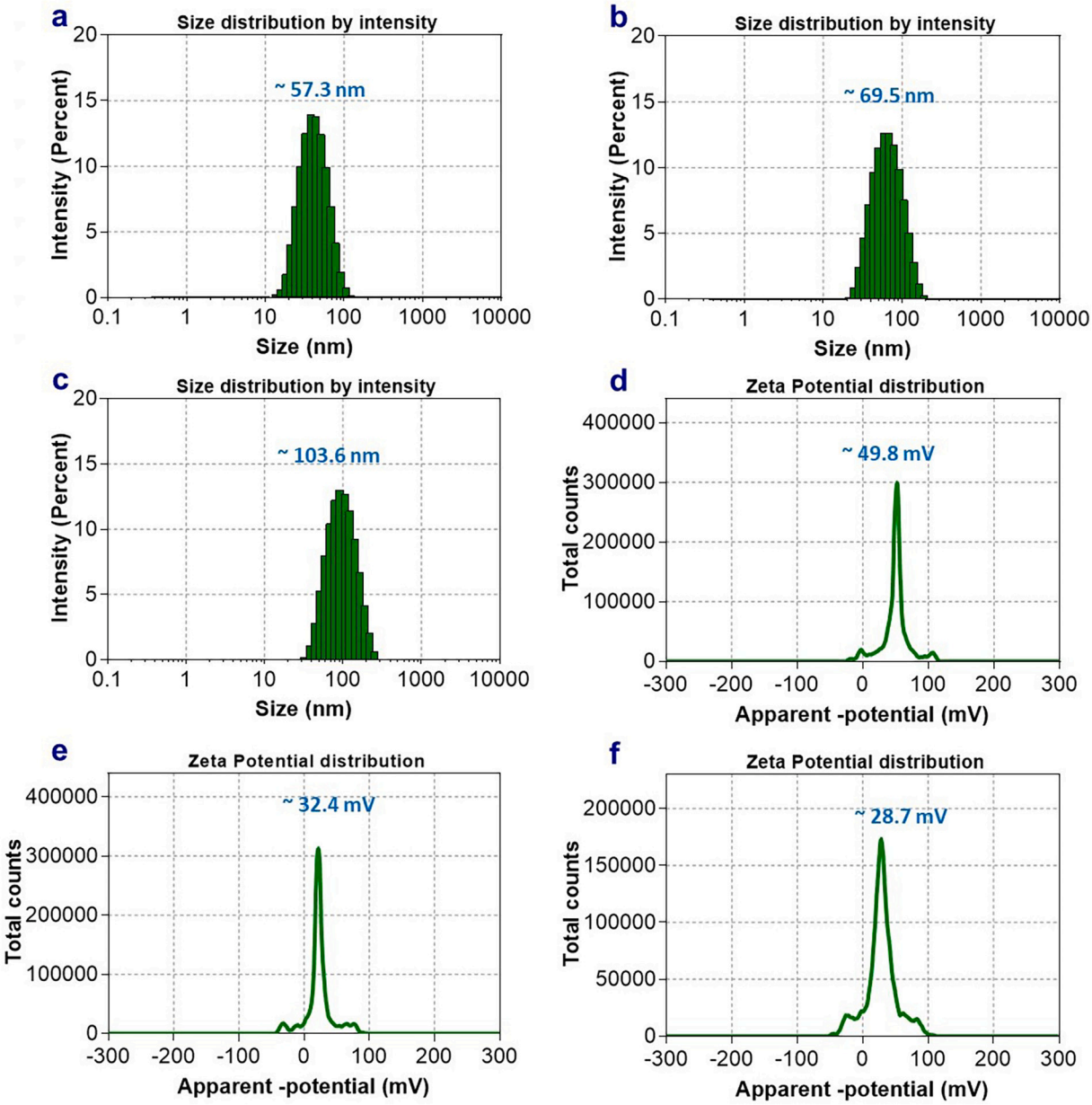

Fig. 5. DLS measurements to show the particle size distribution (hydrodynamic diameter) (a–c) of the developed CS–AgNPs, hybrid NPs I, and hybrid NPs II, respectively. ζ-potential (d–f) of the developed CS–AgNPs, hybrid NPs I, and hybrid NPs II, respectively.

hybrid NPs. The thermal analysis measurements were conducted by differential scanning calorimetry (DSC; Q20, TA Instruments, USA). For that, 5 mg of each sample was heated up to 400 °C at the rate of 10 °C/min in the presence of nitrogen as an inert carrier gas flowing over a rate of 25 mL/min. The thermal behavior of samples was also studied using thermogravimetric analysis (TGA) (Q500, Thermoscientific, USA) with dry nitrogen purge. The change in weight of the samples was determined as a function of temperature. About 5 mg of each sample was heated from room temperature to 600 °C at a rate of 10 °C/min and with nitrogen at a flow rate of 20 mL/ min.

2.4. The encapsulation efficiency % (EE%)

The entrapment efficiency of GA in NPs was evaluated as previously reported [28]. EE% assay was performed by measuring the amount of free drug in the supernatant after ultracentrifugating and concentration of GA was quantified from absorbance of the solution at 269 nm. EE% value was calculated as in Eq. (1) [32]:

$$EE\% = \left[\left(GA_{tot} - GA_{free}\right)/GA_{tot}\right] \times 100 \quad (1)$$

where, GA_{tot} is the mass of GA used for preparation of NPs and GA_{free} is mass of free GA measured in the supernatant.

2.5. ABTS radical cation decolorization assay

The antioxidant power of hybrid-NPs was characterized by ABTS radical cation ($ABTS^{\bullet+}$) decolorization assay [33]. First a solution containing $ABTS^{\bullet+}$ was obtained by reacting 10 mL ABTS with 10 mL $K_2S_2O_8$ (6.0×10^{-5}mol/L) in water.

$$ABTS + S_2O_8^{2-} \rightarrow ABTS^{\bullet} + SO_4^{\bullet-} + SO_4^{2-} \quad (2)$$

The mixture was allowed to stand in dark at room temperature for 48 h before use it. The UV–Vis absorbance spectrum of it was constant for more than two days, reflecting the radical cation $ABTS^{\bullet+}$ kept stable

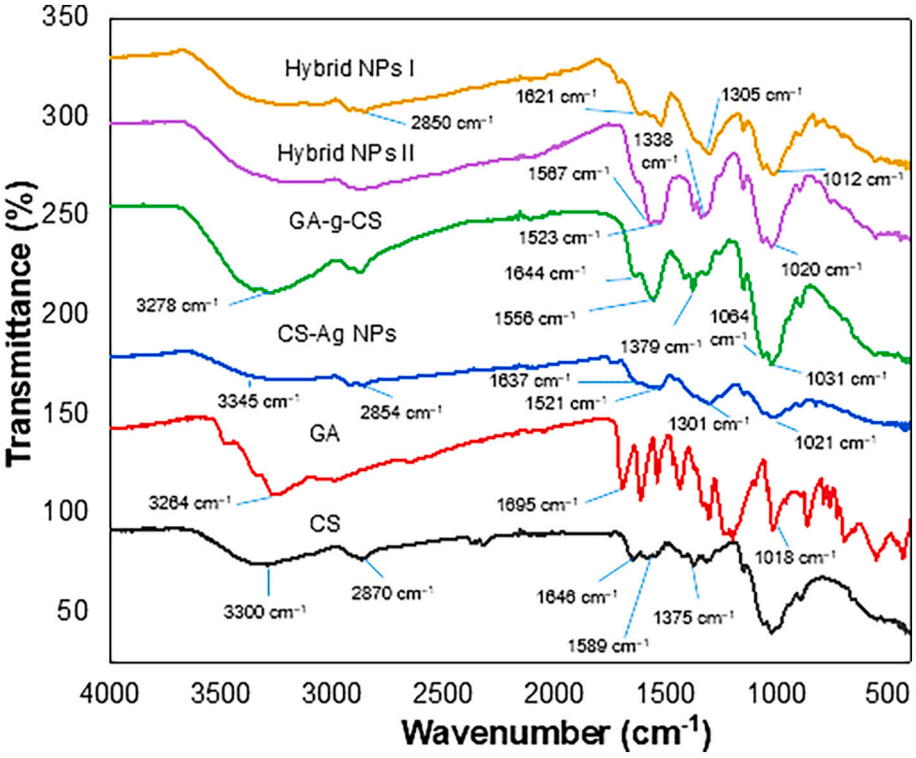

Fig. 6. FTIR of the hybrid NPs.

during that time. These species show three clear peaks between 600 and 900 nm, although the signal at 734 nm was selected to characterize the antioxidant activity of the hybrid NPs, according to the bibliography. The preformed $ABTS^{\bullet+}$ species can be reduced in presence of antioxidants, resulting in reducing its concentration and a consequent decrease of the absorbance of the solution. Different aliquots of NPs solutions were mixed with $ABTS^{\bullet+}$ (3 mL) and UV–Vis spectra were recorded after 6 min [33]. Accordingly, inhibition% after each addition of sample volume was calculated as follows:

$$\text{Inhibition}\% = [(A_b - A)/A_b]^*100 \quad (3)$$

where A_b and A are absorbance at $\lambda = 734$ nm of the original $ABTS^{\bullet+}$ solution and after adding each volume of samples.

Finally, the % inhibition-values were plotted versus the added volume of NPs in order to evaluate their antioxidant activities.

2.6. Assessment of the antibacterial activity

Minimum inhibitory concentration (MIC) and minimum bactericidal concentration (MBC) of hybrid NPs against *Staphylococcus aureus* (strain-COL) and *Escherichia coli* (ATCC 25922) were evaluated using broth microdilution assay [34]. Bacterial cultures were standardized to 0,5McFarland (5×10^7 CFU/mL) in Muller–Hinton Broth. Then, 100 μL of 100-fold diluted inoculants mixed with 100 μL of diluted NPs were incubated (24 h, 37 °C) to indicate MIC. Then, 100 μL of samples without apparent growth were spotted onto MH plates and incubated (24 h, 37 °C) to indicate MBC. Effect of hybrid NPs on bacterial growth kinetics was measured with time killing assay. Growth of 0,5McFcultures treated with MBC of NPs for 0.0,0.5,1,2,4,8 and 24 h was measured by CFU/mL enumeration.

The antibiofilm activity was evaluated as reported previously [35]. *S. aureus* and *E. coli* biofilms were cultured in Tryptic-Soy Broth with 1 % glucose or 8-times diluted Luria Broth respectively. Bacterial cultures adjusted to 0,5McF were added to 96-well plates and incubated (4 h, 37 °C). Then medium was discarded, wells filled with fresh medium and incubated (20 h, 37 °C). Biofilm cultures were washed with PBS, then appropriate broth with MBC of NPs was added. After incubation (24 h, 37 °C) biofilms were washed thrice with PBS. Fresh medium was added and plates were sonicated (10 min, 720 W, 50 Hz). Each sample was serially diluted, spotted on TSA plates for CFU/mL enumeration.

2.7. Mechanism of biocidal action

S. aureus and *E. coli* cells (5×10^7 CFU/mL) treated with NPs for 3 h were harvested by centrifugation and washed thrice with PBS. Samples were fixed with 3 % (*v*/v) glutaraldehyde (1 h), washed in 0.1 mol Soerensen's phosphate buffer (Merck, Germany) (15 min), and dehydrated by incubating in ascending ethanol series (30, 50, 70, 90, and 100 %) for 10 min each. Samples were dried in liquid CO_2 and coated with a 10 nm gold/palladium. Samples were analyzed using SEM (ESEM-XL 30 FEG, FEI, Philips-Netherlands).

2.8. Cytotoxicity assessment

Cytotoxicity of NPs was evaluated on adipose-derived mesenchymal stem cells (ADMSC, ATCC-PCS-500-011) using 3-(4,5-Dimethylthiazol-2-yl)-2,5-diphenyl-2H-tetrazoliumbromide (MTT) assay. Cells were cultured in Dulbecco's Modified Eagle's Medium. Film samples were placed in wells (96-well plate), and MSCs with a density of 1×10^5 cells cm^{-2} were seeded on their surface. Cells were incubated with the samples (24 h, 37 °C, 5 % CO_2) The films and medium were removed and the cells were washed thrice with PBS. Then, MTT solution (5 mg/mL) was added to each well, and the plates were incubated (3 h, 37 °C). Finally, MTT solution was removed, and formazan crystals were dissolved in dimethyl sulfoxide. Optical density was measured using a microplate reader spectrophotometer (Kayto RT-2100C). Fluorescence imaging was performed to show the cells growth and distribution using DAPI (4′,6-diamidino-2-phenylindole) staining method. Images were taken by a fluorescence inverted microscope (Leica).

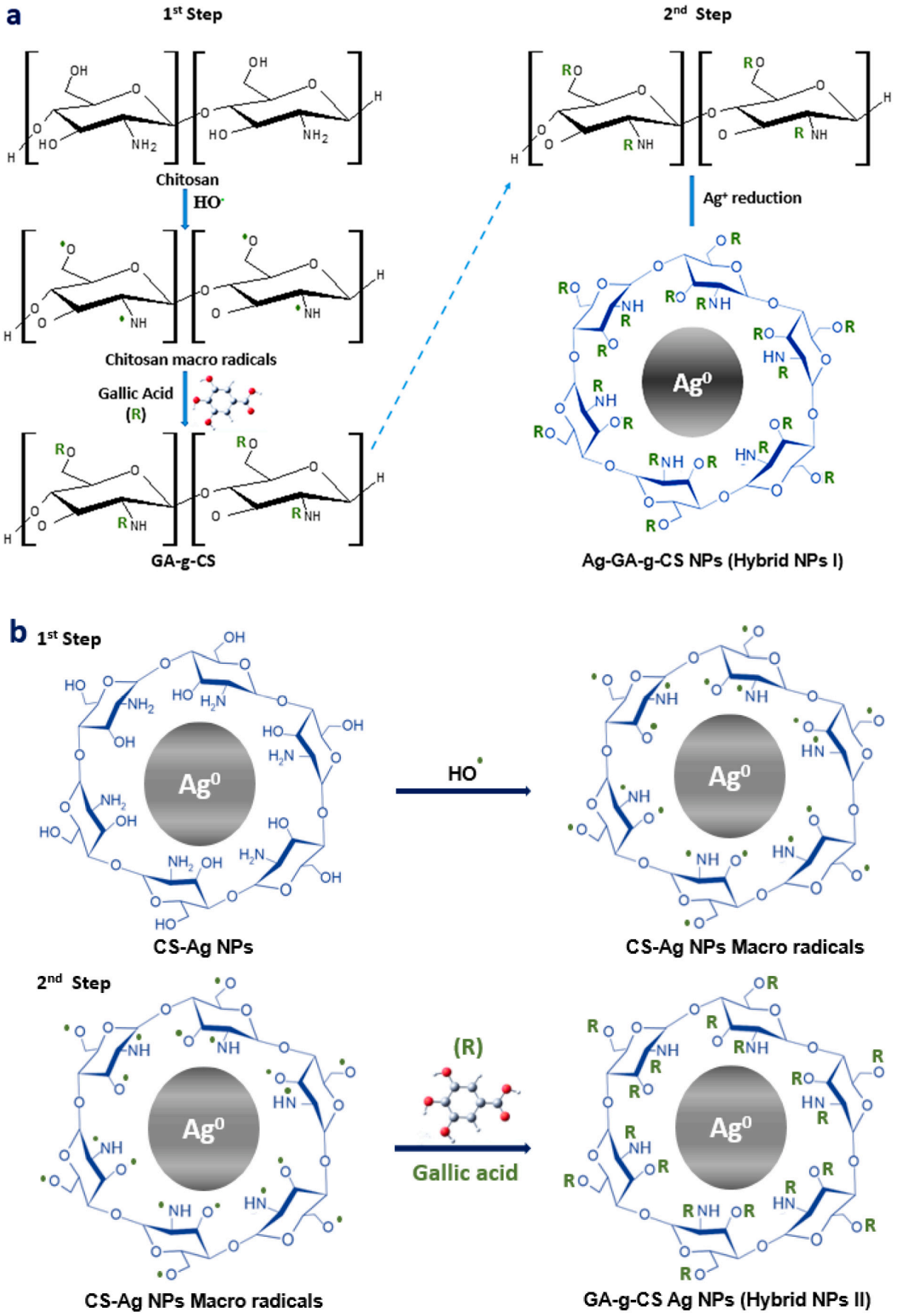

Fig. 7. The schematic illustration of the developed hybrid NPs I (a) and hybrid NPs II (b).

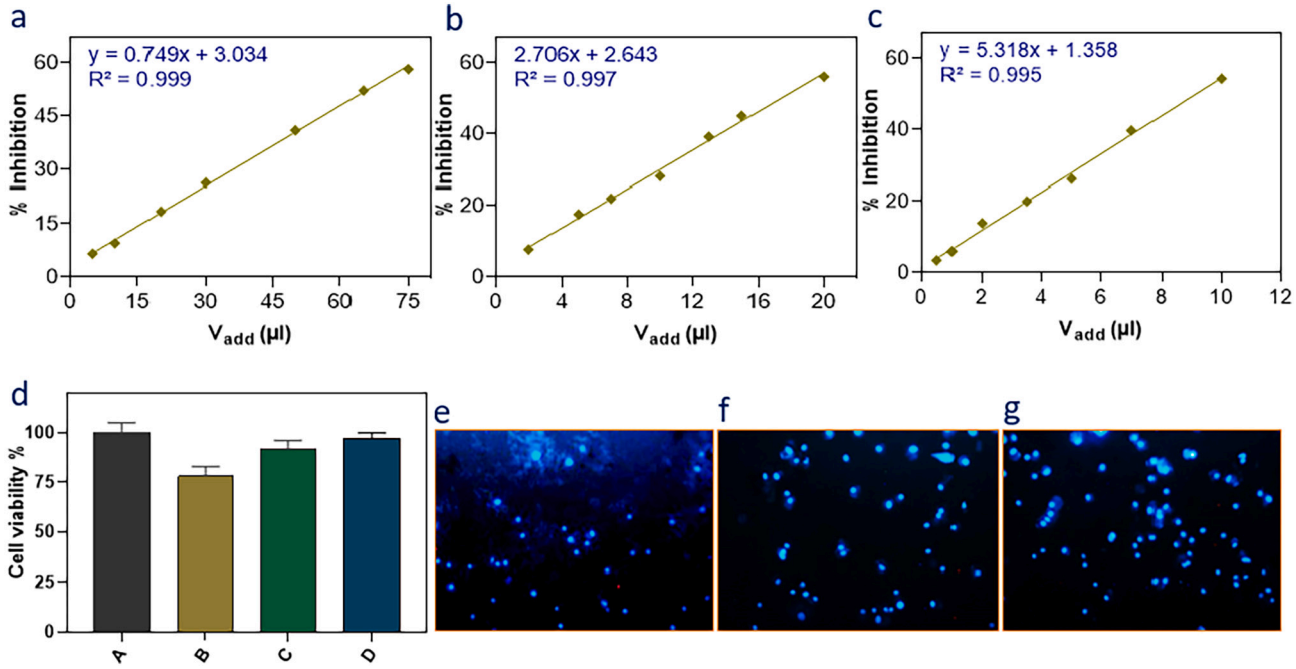

Fig. 8. The antioxidant properties (a–c) of the CS–AgNPs, hybrid NPs I and hybrid NPs II, respectively. Cytotoxic study to show cell viability using MTT assay (d), where A, B, C, and D refer to control, CS-AgNPs, hybrid NPs I and hybrid NPs II, respectively. Cell fluorescent images (e–g) to show cells proliferation and distribution in the presence of CS–AgNPs, hybrid NPs I and hybrid NPs II, respectively.

2.9. Statistical analysis

The results were analyzed using GraphPad Prism 8 software (version 8.02). The statistical significance was evaluated by one-way ANOVA, with a *p*-value used to indicate the significance.

3. Results and discussion

3.1. Optical study

UV spectra were recorded to confirm the grafted GA either to CS or in CS–AgNPs, and to confirm synthesis of AgNPs. UV–Vis spectrum of GA-g-Cs (Fig. 1) shows presence of absorption peak at 271 nm assigned to aromatic region of GA polyphenol [36]. Such absorption band related to GA was also observed in hybrid NPs I and II. UV spectrum of CS–AgNPs displayed a characteristic surface plasmon resonance at 409 nm, which confirmed AgNPs formation. Such band was red-shifted to 423 nm when GA was grafted to CS–AgNPs in hybrid NPs II. Meanwhile, when GA-g-CS was used as reducing/capping agents for AgNPs formation in hybrid NPs I, absorption band red-shifted to 436 nm.

3.2. Electron microscopic imaging and EDX analysis

The morphology of the synthesized hybrid NPs was examined with SEM. As can be observed from Fig. 2, the hybrid NPs appear as spherical particles. EDX-spectra was performed to confirm the composition of the produced hybrid AgNPs. Signals appeared at 3.0 keV in tested NPs, indicate presence of metallic crystalline AgNPs, as in previous studies [37,38]. TEM imaging was carried out to investigate the shape and size of the developed hybrid NPs. The images in Fig. 3 show that the NPs prepared in all cases were spherical in shape with smooth surfaces. According to histograms (Fig. 3d–f), average particle sizes are 12.9 ± 4.1, 63.4 ± 10.1 and 29.7 ± 6.2 nm for CS–AgNPs, hybrid NPs I and II, respectively. Occupied chitosan chains NH_2 and OH, as a result of inserted GA in GA–g–CS, might decrease the reducing capacity of GA–g–CS and lead to relatively bigger nano-sized particles. Where, using redox initiator reaction to CS–AgNPs creates macro-radicals with many binding sites which grafted GA, where the developed hybrid NPs II increased slightly to ~29.7 nm.

3.3. XRD, DSC and TGA

As can be observed in Fig. 4b, XRD patterns, depicting four characteristic diffraction peaks of AgNPs which are assigned to the (111), (200), (220) and (311) crystallographic planes of face-centered cubic (fcc) AgNPs (Joint committee on powder diffraction standards [JCPDS] card number 07-0783) [37]. In Fig. 4a, it can also be observed the presence of the characteristic peak of CS at 22.78° for CS–AgNPs, that was altered, after grafting of GA in either GA-g-CS, hybrid NPs I or II, which confirms the successful grafting GA. Furthermore, all peaks of GA were disappeared after graft in GA-g-CS, hybrid NPs, indicating its successful graft.

DSC of the developed NPs was performed. As shown in Fig. 4c, DSC of GA shows two endothermic peaks. The first one is recorded at 121 °C and attributed to water loss, whereas the second peak observed at 276 °C, is attributed to melting of GA crystal structure [39,40]. CS displays an endothermic peak at 65–115 °C and an exothermic peak at 327 °C, attributed to its thermal decomposition (Hussein et al.). In GA-g-CS, the endothermic and exothermic peaks appeared at 83 °C and 293 °C, respectively. In hybrid NPs I, the endothermic peak increased to 102 °C, while the exothermic peak decreased to 276 °C. Meanwhile, hybrid NPs II showed an increase in both endothermic and exothermic peaks to 96 °C and 300 °C, respectively. Although GA showed a characteristic peak at 276 °C, this peak diminished or almost disappeared in DSC curves of GA-g-CS, hybrid NPs I and II. According to previous studies [41,42], this indicates that the grafted GA lost its original crystalline structure and consequent encapsulation of GA. The enthalpic peak related to GA diminished when GA grafted to CS in GA-g-CS and in hybrid NPs I, disappearing completely when GA was grafted to CS–AgNPs in hybrid NPs II. This can be attributed to complexation of GA with macro-radicals CS–AgNPs.

TGA was carried out Fig. 4(d,e). The thermal degradation of GA occurs through a three-step temperature range, with 24.6 % of the sample weight being left at 600 °C. The temperature at which the first

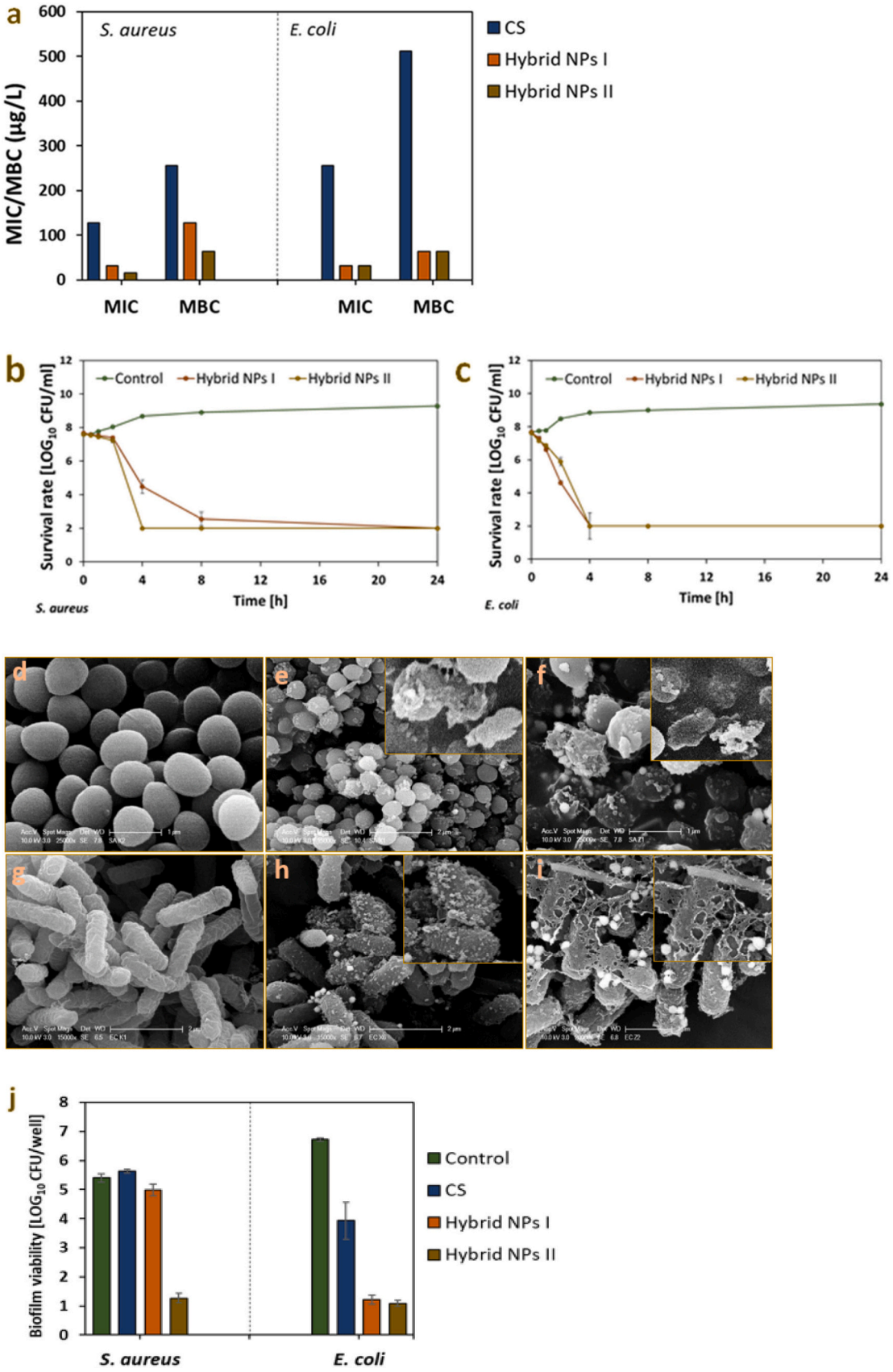

Fig. 9. Antibacterial activity of the tested hybrid NPs using MIC/MBC (a), and time killing assay (b – *S. aureus*, c – *E. coli*). SEM imaging showing control, hybrid NPs I and hybrid NPs II effect against *S. aureus* (d–f), and and *E. coli* (g–i), respectively. The insets show damaged bacterial cells with ruptured morphology and formation of pits and holes on the bacterial surface. Antibiofilm activity of the tested hybrid NPs (j).

and the second degradation steps take place was 140 and 250 °C, respectively. Thereafter, the final third step of weight loss occurred in range 380-600 °C. Though both CS and CS–AgNPs films exhibited similar degradation patterns, however, the final mass loss occurred in CS–AgNPs was less than CS. The first degradation step, observed in the range 50-264 °C for CS and 55-271 °C for CS–AgNPs, is assigned to evaporation of water and glycerin molecules. The second step of weight loss occurs at 265-415 °C for CS and 240-472 °C for CS–AgNPs. Final mass loss of CS occurs throughout a complex series of degradation processes up to 600 °C, which ends with oxidative degradation of carbonaceous residues [43,44]. The delay observed in the degradation throughout the second step for CS–AgNPs is ascribed to presence of Ag.

In TGA curves of GA-g-CS and hybrid NPs I, first weight loss took place at 57-192 °C, and 38-198 °C, respectively. The second weight loss step is observed at 192-334 and 198-402 °C for GA-g-CS and hybrid NPs I, respectively. Both GA-g-CS and hybrid NPs I displayed lowest residual amount left over (28 and 30 %, respectively). This could be attributed to the grafted GA, where CS losses its packing chain structure [41]. Hybrid NPS II showed delayed degradation compared to hybrid NPs I. The residual amounts left over in CS–AgNPs and hybrid NPs II were ~36 and 34 % respectively. The higher stability of CS-AgNPs and hybrid NPs, can be claimed to the complexation which takes place between CS with the surface of AgNPs in CS–AgNPs, and complexation of the grafted GA to CS-AgNPs in hybrid NPs II.

3.4. Particle size distribution and ζ-potential of the hybrid NPs

The particle size distribution and ζ-potential of the synthesized NPs were measured with DLS (Fig. 5). CS-AgNPs exhibited a hydrodynamic diameter 57 nm. Hybrid NPs I, presented 103 nm. Meanwhile, hybrid NPs II displayed ~69 nm. ζ-potential value of CS-AgNPs was around +49.8 mV because of the positively charged amine groups. It is observed that ζ-potential of CS-AgNPs decreased with the grafted GA, as in GA-g-CS AgNPs (hybrid NPs I), where it decreased to +32 mV. This can be illustrated as GA molecules strongly interfere in the net charge of obtained particles when used as reducing/capping agent simultaneously with CS. Meanwhile, in hybrid NPs II, GA molecules shown a higher effect on the net charges of AgNPs (~+28 mV). Even with such low ζ-potential, the stability was still good. ζ-potential values above 25 mV are associated to a good stability [28]. The produced AgNPs by Lunkov et al., (2020) showed low ζ-potential (+8 mV), as a result of performing the reaction at pH 7.5 which considered non-desirable for CS and CS-NPs in the aspects of their solubility and cationic ζ-potential where they are likely to aggregate [20,21]. This can be attributed to two forces: presence of CS which combines both electrostatic and steric stabilizations due to its positive charge and its polymeric nature respectively [28], and the complexation power happened between the inserted GA to CS-AgNPs macro-radicals.

3.5. FTIR

Fig. 6 shows IR spectra for pure-CS, GA, GA-g-CS, CS–AgNPs, hybrid NPs I and II. The characteristic IR absorption band of CS, which is attributed to stretching of O—H and NH_2, was observed at 3300 cm^{-1}. The absorbance peak at 2870 cm^{-1} corresponds to C—H stretching vibrations. The peaks at 1646, 1589 and 1375 cm^{-1} are associated with stretching vibrations of amide I, amide II and amide III, respectively [16].

For GA, the bands at 3100 cm^{-1} to 3800 cm^{-1} can be attributed to –OH stretching and hydrogen bonds between phenolic hydroxyl groups. The peak at 1695 cm^{-1} is assigned to absorption of carboxylic group. The bands due to bending vibrations of C—H in and O—H of the phenol alcohol appeared at 1332–1018 cm^{-1} [42,45]. For CS–AgNPs, the shift and the decrease in the intensity of the CS peak which is attributed to the stretching of O—H and NH_2, were noticed by the addition of $AgNO_3$ (Ag^+), due to the interaction of the reduced Ag^0 with CS chains. Furthermore, most of the peaks of CS shifted and changed in intensity as a result of the AgNPs formation [24,46].

As a result of inserting GA into CS chain (GA-g-CS), a new band appeared at 1556 cm^{-1} which was assigned to carbon-to-carbon stretching within the GA aromatic ring [40]. Moreover, the CS characteristic peak which is attributed to the stretching of O—H and NH_2, shifted and increased in the intensity. Moreover, the other characteristic peaks of CS at 1375, 1059 and 1024 cm^{-1} increased in intensity, and moved to 1379, 1064 and 1031 cm^{-1}, respectively, as a result of the GA graft with CS. For hybrid NPs II, most of the peaks of CS–AgNPs increased in intensity and shifted, with observed new peaks due to the inserted GA into CS–AgNPs. The complexation of GA with the frequent macro-radicals CS–AgNPs, leaded to broad and shifts of the peaks in GA conjugated CS–AgNPs. On the other hand, the peaks of GA-g-CS at 1644, 1556 and 1379 cm^{-1} decreased in intensity and moved to 1567, 1523 and 1338 cm^{-1} respectively, which took place as a result of using GA-g-CS to reduce Ag in hybrid NPs I.

3.6. Synthesis of the hybrid NPs

Schematic illustration (Fig. 7 a,b) was designated to show the formulation of hybrid NPs I and II. The conjugation of the GA moieties on the CS polymeric backbone was achieved via free radical-induced grafting reaction. The redox initiator reaction system is composed of Vc/H_2O_2 pair, solubilized in water, where H_2O_2 oxidizes ascorbic acid to produce ascorbate and hydroxyl radicals ($HO^•$) which initiate the reaction system. The graft reaction system includes 2 steps; in the first step, the produced ($HO^•$) needs 30 min to form macro-radical through attacking and abstracting hydrogen atom from NH_2, CH_2 and OH groups in CS; and then followed by the second step with addition of GA in reaction system where the inserted GA moieties on CS chains takes place. During the reaction system in the first step, ascorbic acid in the acidic medium reacts with H_2O_2 and undergoes two series of deprotonation with releasing of $HO^•$ [29]. As the pK decreases to −86, the deprotonated form of ascorbic acid has no ability to protonate, and thus the released $HO^•$ continues to initiate the reaction system [29,47]. For the grafted GA on CS–AgNPs, it is hypothesized that the redox initiator reaction is stronger due to present of silver, which allows to generate larger amount of hydroxyl radicals. And thus, enable higher amount of GA to be inserted on CS chains. The other reason which led to inserting higher amount of GA moieties on CS–AgNPs, is the surface to volume of CS-AgNPs macro-radicals compared to CS macro-radicals. The increase in the accumulation of free radicals induced by AgNPs was reported in previous studies. It was reported that the addition of ascorbic acid in acidic medium render it as a diacid form ($AscH_2$) which reacts with H_2O_2 and generates the $HO^•$ [29]. The produced $HO^•$ acts as radical initiator which works through abstracting H atoms from CS chains with formation CS macro-radicals. GA then accepts the macro radicals, and eventually the GA-g-CS is formed. As presented in Fig. 7a, the GA-g-CS was used for the reduction of Ag^+ to Ag^0 with formation of hybrid NPs I. The step of applying the Vc/H_2O_2 redox pair was performed with the prepared CS-AgNPs, then GA was grafted to CS–AgNPs to form GA-g-CS-AgNPs (hybrid NPs II) as shown in Fig. 7b. The presence of hydrogen bonding in CS-AgNPs makes them good substrates to form frequent macro-radicals and to graft high amount of GA. Conjugated GA was evidenced by UV-spectra, FTIR and DSC/TGA.

3.7. Encapsulation efficiency (%) and ABTS radical action decolorization assay (antioxidant activity)

Gallic acid (GA) is considered as a strong antioxidant, offering effective protection against oxidative damage caused by various reactive species found in biological systems [48]. Besides, anti-oxidative properties have been reported for chitosan (CS) [49].

The EE% of GA was crucial for the antioxidant power of the developed NPs. Hybrid NPs II showed higher EE% (~78 %) than hybrid NPs I

(~ 66 %). The antioxidant power of the tested NPs was analyzed by using the ABTS radical cation ($ABTS^{\bullet+}$) assay. As can be seen in Fig. 8a–c, the % inhibition followed a linear variation with the volume of NPs solution in all cases. The data were fitted to a linear curve, finding that the slope of the linear regression increases in the following order: CS–AgNPs > NPs I > NPs II. Thus, it can be confirmed that the antioxidant activity of hybrid-NPs increases by conjugating GA, presenting higher antioxidant capacity compared to CS–AgNPs.

3.8. Cyto-biocompatibility

The biological applications of AgNPs are limited owing to the potential toxicity of silver ions for mammalian cells [50]. The excessive produced ROS by AgNPs leads to oxidative stress associated to oxidative damage to the body biomolecules including lipids and DNA, as well as an increase in the level of the inflammatory response [51,52]. Using CS as stabilizing/capping agent is supposed to minimize such toxic effect. Moreover, the conjugation of GA in CS–AgNPs could alleviate and improve the cytotoxic profile of tested hybrid-NPs. The cell viability was conducted using MTT assay. Fig. 8d shows that hybrid NPs displayed better environment for the cells viability than using CS–AgNPs. In particular, hybrid NPs II displayed higher cell viability endowed to higher content of the encapsulated GA. To confirm this, MSCs were seeded over CS–AgNPs, hybrid NPs I and II films. Fluorescent images were taken, showing that the cells grow and distribute well over hybrid NPs I and II (Fig. 8e–g). In a previous study which used non-ecofriendly carbodiimide coupling-based reaction, the produced chitosan-gallic acid-AgNPs showed a slight cytotoxicity [19], where the employed ecofriendly Vc/H_2O_2 redox pair for producing AgNPs in the current work, evidenced their biocompatibility in particular the produced hybrid-NPs II.

The presence of GA as antioxidant agent (ROS scavenger) with high encapsulated content in hybrid NPs II might play a key role to limit the cytotoxic effect of Ag atoms and, subsequently, could enhance cells to grow efficiently. Hybrid NPs I and II were then tested against microbial strains including *S. aureus* and *E. coli*.

3.9. Antibacterial activity

In MIC/MBC assay both hybrid NPs showed much higher antibacterial activity than CS (Fig. 9a). *E. coli* was more susceptible to hybrid NPs than *S. aureus*, which is attributed to the change in surface charges of hybrid NPs. Also, hybrid NPs II were more effective than hybrid NPs I against *S. aureus*. Time killing assay reflected the potent antibacterial efficiency of hybrid NPs (Fig. 9b-c). *E. coli* was more sensitive to both hybrid NPs than *S. aureus*. Also, for *S. aureus* hybrid NPs II were more effective than hybrid NPs I. For *S. aureus* biofilm there was observed no effect of CS, weak effect of hybrid NPs I and very strong antibacterial effect of hybrid NPs II. For *E. coli* biofilm CS has limited effectiveness, but both hybrid NPs have very potent antimicrobial effects (Fig. 9j).

To investigate the interaction of hybrid NPs with *S. aureus* and *E. coli* cells, SEM imaging was performed (Fig. 9d-i). Non-treated bacterial cells showed smooth and intact structure, whereas the cells subjected to NPs for 3 h treatment, were dramatically damaged, with losing their morphological structure and membrane integrity. *E. coli* cells were damaged with ruptured morphology (inset) and formation of pits and holes. AgNPs were demonstrated to cause irregular pits on bacterial cell wall, allowing NPs to enter the periplasmic space and then into the cell. Such pits formation and morphological changes can be visualized by SEM [53,54]. It is hypothesized that the bacterial surface proteins may facilitate the NPs binding and forming such a peculiar pattern of aggregation which namely AgNPs aggregates [54]. GA insertion on CS-AgNPs boosts the antibacterial effect of the obtained NPs, due to the dual antibacterial action of amine group in CS and polyphenol-based GA along with Ag ions. The previous studies [19] did not evaluate the antibiofilm activity, nor the time of killing or the mechanism of action, which were presented in the current work. Also, CS-GA-AgNPs showed MIC values at 62.5 μg/mL for both *E. coli* and *S. epidermidis* [19], whereas the hybrid NPs II in current study, showed lower MIC against *S. aureus* and *E. coli*. This can be attributed to using pH 7.5 during reaction process which is not desired for CS and CSNPs, in aspects of their solubility and stability (low ζ-potential +8 mV), where they are likely to aggregate which subsequently leads to loss of their antibacterial efficiency [20,21]. Biofilm plays role in pathogenesis of many chronic diseases (i.e. wound, caries). Bacteria grown in biofilm are up to 1000-fold less susceptible to antimicrobial agents what makes it very hard to eradicate [55]. High antibiofilm activity of hybrid NPs II ($>4\log_{10}$ CFU/mL reduction) indicates its great medical potential.

4. Conclusions

In summary, we have developed two approaches to develop CS/GA/Ag in a single nanostructure via free radical-induced grafting reactions. The first method employed the GA-g-CS as reducing/capping agents for Ag atoms and the second one conjugated GA to the pre-prepared CS–AgNPs, giving place to hybrid NPs I and hybrid NPs II, respectively. These NPs were characterized by UV–vis spectra, DLS, XRD, DSA/TGA, FTIR, TEM and SEM-EDX. The results confirmed the successful integration of GA into CS–AgNPs. The decrease in ζ-potential value in hybrid NPs I and II compared to CS-AgNPs was attributed to the presence of GA, which neutralized the cationic CS. According to the DLS and TEM imaging, the hybrid NPs II showed smaller nanoscale than hybrid NPs I. The antioxidant evaluation using ABTS, cyto-biocompatibility and antibacterial activity against *E. coli* and *S. aureus* showed the better impact of hybrid NPs II, owing to the presence of GA and its higher entrapped content. The method developed here to conjugate GA to CS–AgNPs via free radical-mediated reaction using Vc/H_2O_2 redox pair, opens up a new direction in the synthesis of surface functionalized nanomaterials. It has proved its efficiency as potent antioxidant and antimicrobial agents, in addition to its safety for humans. Thus, the synthesized hybrid NPs could be promising candidates to be integrated into bone and wound dressing mats.

CRediT authorship contribution statement

Mohamed A. Mohamady Hussein: Conceptualization, Methodology, Investigation, Software, Data curation, Visualization, Writing - Original draft preparation. **José Manuel Olmos:** Methodololgy, Validation, Investigation, software, Writing—review & editing. **Michał K. Pierański:** Methodology, Validation, Investigation, software, Writing—review and editing. **Mariusz Grinholc:** Methodology, Resources, Writing- Reviewing and Editing. **Eva Miriam Buhl:** Investigation, Writing- Reviewing and Editing. **Oguzhan Gunduz:** Resources, Writing-Reviewing and Editing. **Ahmed M. Youssef:** Investigation, Visualization, software. **Carlos M. Pereira:** Resources, Writing- Reviewing and Editing. **Ibrahim M. El-Sherbiny:** Validation, Writing- Reviewing and Editing. **Mosaad Megahed:** Supervision, Resources, Project administration, Visualization, Writing—review and editing.

Declaration of competing interest

The authors declare that they have no known competing financial interests or personal relationships that could have appeared to influence the work reported in this paper.

Acknowledgement

The authors are grateful to Islamic Development Bank (IDB), Jeddah, Saudi Arabia, for financially supporting this work through the IDB Merit Scholarship Program (Ref. 36/11207330, File No.23/EGT/P34). The antioxidant assessments were covered by FCT under Research Grant UIDB/00081/2020–CIQUP and by a grant for postdoctoral training

funded by Counseling of Employment, Business and Environment of the CARM, through Seneca Foundation-Agency of Science and Technology of Murcia Region.

References

[1] P.D. Ray, B.-W. Huang, Y. Tsuji, Reactive oxygen species (ROS) homeostasis and redox regulation in cellular signaling, Cell. Signal. 24 (2012) 981–990, https://doi.org/10.1016/j.cellsig.2012.01.008.

[2] A. Hashkavayi, S. Hashemnia, S. Osfouri, S. Zarei, Electrochemical study of antioxidant capacity of Gracilaria pygmaea macro-algae based on the green synthesis of gold nanoparticles: assessment of its cytotoxic effect on four cancer cell lines, J. Electrochem. Soc. 166 (2019) B969–B977, https://doi.org/10.1149/2.0951912jes.

[3] C. Pansara, R. Mishra, T. Mehta, A. Parikh, S. Garg, Formulation of chitosan stabilized silver nanoparticle-containing wound healing film: in-vitro and in-vivo characterization, J. Pharm. Sci. 109 (2020), https://doi.org/10.1016/j.xphs.2020.03.028.

[4] S. Nakamura, M. Sato, Y. Sato, N. Ando, T. Takayama, M. Fujita, M. Ishihara, Synthesis and application of silver nanoparticles (Ag NPs) for the prevention of infection in healthcare workers, Int. J. Mol. Sci. 20 (2019) 3620, https://doi.org/10.3390/ijms20153620.

[5] M. Stensberg, Q. Wei, E. Mclamore, D. Porterfield, A. Wei, M. Sepulveda, Toxicological studies on silver nanoparticles: challenges and opportunities in assessment, monitoring and imaging, Nanomedicine 6 (2011) 879–898, https://doi.org/10.2217/nnm.11.78 (Lond).

[6] M.F. Queiroz, D.A. Sabry, G.L. Sassaki, H.A.O. Rocha, L.S. Costa, Gallic acid-dextran conjugate: green synthesis of a novel antioxidant molecule, Antioxidants 8 (2019) 478, https://doi.org/10.3390/antiox8100478 (Basel, Switzerland).

[7] J. Chao, T.-I. Huo, H.-Y. Cheng, J.-C. Tsai, J.-W. Liao, M.-S. Lee, X.-M. Qin, M.-T. Hsieh, L.-H. Pao, W.-H. Peng, Gallic acid ameliorated impaired glucose and lipid homeostasis in high fat diet-induced NAFLD mice, PLoS One 9 (2014), https://doi.org/10.1371/journal.pone.0096969 e96969-e96969.

[8] Y. Deligiannakis, G.A. Sotiriou, S.E. Pratsinis, Antioxidant and antiradical SiO2 nanoparticles covalently functionalized with gallic acid, ACS Appl. Mater. Interfaces 4 (2012) 6609–6617, https://doi.org/10.1021/am301751s.

[9] S. Bhattacharyya, S.M. Ahammed, B.P. Saha, P.K. Mukherjee, The gallic acid-phospholipid complex improved the antioxidant potential of gallic acid by enhancing its bioavailability, AAPS PharmSciTech 14 (2013) 1025–1033, https://doi.org/10.1208/s12249-013-9991-8.

[10] S. Shahrzad, K. Aoyagi, A. Winter, A. Koyama, I. Bitsch, Pharmacokinetics of gallic acid and its relative bioavailability from tea in healthy humans, J. Nutr. 131 (2001) 1207–1210, https://doi.org/10.1093/jn/131.4.1207.

[11] J. Lee, K.-H. Choi, J. Min, H.-J. Kim, J.-P. Jee, B.J. Park, Functionalized ZnO nanoparticles with gallic acid for antioxidant and antibacterial activity against methicillin-resistant S. aureus, Nanomaterials 7 (2017) 365, https://doi.org/10.3390/nano7110365 (Basel, Switzerland).

[12] M.W. Abebe, R. Appiah-Ntiamoah, H. Kim, Gallic acid modified alginate self-adhesive hydrogel for strain responsive transdermal delivery, Int. J. Biol. Macromol. 163 (2020) 147–155, https://doi.org/10.1016/j.ijbiomac.2020.06.257.

[13] H.-H. Park, S.-C. Ko, G.-W. Oh, Y.-M. Jang, Y.-M. Kim, W.S. Park, I.-W. Choi, W.-K. Jung, Characterization and biological activity of PVA hydrogel containing chitooligosaccharides conjugated with gallic acid, Carbohydr. Polym. 198 (2018) 197–205, https://doi.org/10.1016/j.carbpol.2018.06.070.

[14] M. Hussein, S. Ulağ, A. Abo Dena, A. Sahin, M. Grinholc, O. Gunduz, I. El-Sherbiny, M. Megahed, Chitosan/gold hybrid nanoparticles enriched electrospun PVA nanofibrous mats for the topical delivery of Punica granatum L. extract: synthesis, characterization, biocompatibility and antibacterial properties, Int. J. Nanomedicine 16 (2021) 5133–5151, https://doi.org/10.2147/IJN.S306526.

[15] A. Abruzzo, G. Zuccheri, F. Belluti, S. Provenzano, L. Verardi, F. Bigucci, T. Cerchiara, B. Luppi, N. Calonghi, Chitosan nanoparticles for lipophilic anticancer drug delivery: development, characterization and in vitro studies on HT29 cancer cells, Colloids Surf.B Biointerfaces 145 (2016) 362–372, https://doi.org/10.1016/j.colsurfb.2016.05.023.

[16] M.A. Mohamady Hussein, F.G.D. Baños, M. Grinholc, A.S. Abo Dena, I.M. El-Sherbiny, M. Megahed, Exploring the physicochemical and antimicrobial properties of gold-chitosan hybrid nanoparticles composed of varying chitosan amounts, Int. J. Biol. Macromol. (2020), https://doi.org/10.1016/j.ijbiomac.2020.08.046.

[17] T. Tayebi, A. Baradaran-Rafii, A. Hajifathali, A. Rahimpour, H. Zali, A. Shaabani, H. Niknejad, Biofabrication of chitosan/chitosan nanoparticles/polycaprolactone transparent membrane for corneal endothelial tissue engineering, Sci. Rep. 11 (2021) 7060, https://doi.org/10.1038/s41598-021-86340-w.

[18] P. Nezhad-Mokhtari, M. Akrami-Hasan-Kohal, M. Ghorbani, An injectable chitosan-based hydrogel scaffold containing gold nanoparticles for tissue engineering applications, Int. J. Biol. Macromol. 154 (2020) 198–205, https://doi.org/10.1016/j.ijbiomac.2020.03.112.

[19] A. Lunkov, B. Shagdarova, M. Konovalova, Y. Zhuikova, N. Drozd, A. Il'ina, V. Varlamov, Synthesis of silver nanoparticles using gallic acid-conjugated chitosan derivatives, Carbohydr. Polym. 234 (2020), 115916, https://doi.org/10.1016/j.carbpol.2020.115916.

[20] S.-H. Chang, H.-T.V. Lin, G.-J. Wu, G.J. Tsai, pH effects on solubility, zeta potential, and correlation between antibacterial activity and molecular weight of chitosan, Carbohydr. Polym. 134 (2015) 74–81, https://doi.org/10.1016/j.carbpol.2015.07.072.

[21] D.S. Freitas, P. Teixeira, I.B. Pinheiro, E.M.S. Castanheira, P.J.G. Coutinho, M. J. Alves, Chitosan nano/microformulations for antimicrobial protection of leather with a potential impact in tanning industry, Materials 15 (2022), https://doi.org/10.3390/ma15051750.

[22] J. Liu, H. Pu, S. Liu, J. Kan, C. Jin, Synthesis, characterization, bioactivity and potential application of phenolic acid grafted chitosan: a review, Carbohydr. Polym. 174 (2017) 999–1017, https://doi.org/10.1016/j.carbpol.2017.07.014.

[23] Y. Diao, X. Yu, C. Zhang, Y. Jing, Quercetin-grafted chitosan prepared by free radical grafting: characterization and evaluation of antioxidant and antibacterial properties, J. Food Sci. Technol. 57 (2020) 2259–2268, https://doi.org/10.1007/s13197-020-04263-2.

[24] S. Kumar-Krishnan, E. Prokhorov, M. Hernández-Iturriaga, J.D. Mota-Morales, M. Vázquez-Lepe, Y. Kovalenko, I.C. Sanchez, G. Luna-Bárcenas, Chitosan/silver nanocomposites: synergistic antibacterial action of silver nanoparticles and silver ions, Eur. Polym. J. 67 (2015) 242–251, https://doi.org/10.1016/j.eurpolymj.2015.03.066.

[25] K. Li, G. Guan, J. Zhu, H. Wu, Q. Sun, Antibacterial activity and mechanism of a laccase-catalyzed chitosan–gallic acid derivative against Escherichia coli and Staphylococcus aureus, Food Control 96 (2019) 234–243, https://doi.org/10.1016/j.foodcont.2018.09.021.

[26] M. Zheng, C. Zhang, Y. Zhou, H. Zhao, X. Bie, F. Lu, Preparation of gallic acid-grafted chitosan using recombinant bacterial laccase and its application in chilled meat preservation, Front. Microbiol. 9 (2018), https://doi.org/10.3389/fmicb.2018.01729.

[27] K. Nemčeková, V. Svitková, J. Sochr, P. Gemeiner, J. Labuda, Gallic acid-coated silver nanoparticles as perspective drug nanocarriers: bioanalytical study, Anal. Bioanal. Chem. (2022), https://doi.org/10.1007/s00216-022-03955-2.

[28] J. Lamarra, S. Rivero, A. Pinotti, Design of chitosan-based nanoparticles functionalized with gallic acid, Mater. Sci. Eng. C 67 (2016) 717–726, https://doi.org/10.1016/j.msec.2016.05.072.

[29] J. Liu, J. Lu, J. Kan, C. Jin, Synthesis of chitosan-gallic acid conjugate: structure characterization and in vitro anti-diabetic potential, Int. J. Biol. Macromol. 62 (2013) 321–329, https://doi.org/10.1016/j.ijbiomac.2013.09.032.

[30] L. Dai, B. Nadeau, X. An, D. Cheng, Z. Long, Y. Ni, Silver nanoparticles-containing dual-function hydrogels based on a guar gum-sodium borohydride system, Sci. Rep. 6 (2016) 36497, https://doi.org/10.1038/srep36497.

[31] A. Shah, I. Hussain, G. Murtaza, Chemical synthesis and characterization of chitosan/silver nanocomposites films and their potential antibacterial activity, Int. J. Biol. Macromol. 116 (2018) 520–529, https://doi.org/10.1016/j.ijbiomac.2018.05.057.

[32] R. Pulicharla, C. Marques, R.K. Das, T. Rouissi, S.K. Brar, Encapsulation and release studies of strawberry polyphenols in biodegradable chitosan nanoformulation, Int. J. Biol. Macromol. (2016), https://doi.org/10.1016/j.ijbiomac.2016.03.036.

[33] R. Re, N. Pellegrini, A. Proteggente, A. Pannala, M. Yang, C. Rice-Evans, Antioxidant activity applying an improved ABTS radical cation decolorization assay, Free Radic. Biol. Med. 26 (1999) 1231–1237, https://doi.org/10.1016/S0891-5849(98)00315-3.

[34] C.A. Marangon, V.C.A. Martins, M.H. Ling, C.C. Melo, A.M.G. Plepis, R.L. Meyer, M. Nitschke, Combination of rhamnolipid and chitosan in nanoparticles boosts their antimicrobial efficacy, ACS Appl. Mater. Interfaces 12 (2020) 5488–5499, https://doi.org/10.1021/acsami.9b19253.

[35] M.K. Pieranski, M. Rychlowski, M. Grinholc, Optimization of Streptococcus agalactiae biofilm culture in a continuous flow system for photoinactivation studies, Pathogens 10 (2021), https://doi.org/10.3390/pathogens10091212.

[36] E.H. Anouar, J. Gierschner, J.-L. Duroux, P. Trouillas, UV/visible spectra of natural polyphenols: a time-dependent density functional theory study, Food Chem. 131 (2012) 79–89, https://doi.org/10.1016/j.foodchem.2011.08.034.

[37] M.A. Mohamady Hussein, E. Guler, E. Rayaman, M.E. Cam, A. Sahin, M. Grinholc, D. Sezgin, Y.M. Sahin, O. Gunduz, M. Muhammed, I.M. El-Sherbiny, M. Megahed, Dual-drug delivery of Ag-chitosan nanoparticles and phenytoin via core-shell PVA/PCL electrospun nanofibers, Carbohydr. Polym. (2021), 118373, https://doi.org/10.1016/j.carbpol.2021.118373.

[38] H.M. Fahmy, A. Aly, A. Abou-okeil, A non-woven fabric wound dressing containing layer – by – layer deposited hyaluronic acid and chitosan, Int. J. Biol. Macromol. 114 (2018), https://doi.org/10.1016/j.ijbiomac.2018.03.149.

[39] C.G. da Rosa, C.D. Borges, R.C. Zambiazi, M.R. Nunes, E.V. Benvenutti, S.R. da Luz, R.F. D'Avila, J.K. Rutz, Microencapsulation of gallic acid in chitosan, β-cyclodextrin and xanthan, Ind. Crop. Prod. 46 (2013) 138–146, https://doi.org/10.1016/j.indcrop.2012.12.053.

[40] M. Curcio, F. Puoci, F. Iemma, O.I. Parisi, G. Cirillo, U.G. Spizzirri, N. Picci, Covalent insertion of antioxidant molecules on chitosan by a free radical grafting procedure, J. Agric. Food Chem. 57 (2009) 5933–5938, https://doi.org/10.1021/jf900778u.

[41] J. Liu, X. Wen, J. Lu, J. Kan, C. Jin, Free radical mediated grafting of chitosan with caffeic and ferulic acids: structures and antioxidant activity, Int. J. Biol. Macromol. 65 (2014) 97–106, https://doi.org/10.1016/j.ijbiomac.2014.01.021.

[42] P. Thangavel, B. Ramachandran, V. Muthuvijayan, Fabrication of chitosan/gallic acid 3D microporous scaffold for tissue engineering applications, J. Biomed. Mater. Res. B Appl. Biomater. 104 (2016) 750–760, https://doi.org/10.1002/jbm.b.33603.

[43] G.M. Raghavendra, J. Jung, D. Kim, J. Seo, Microwave assisted antibacterial chitosan–silver nanocomposite films, Int. J. Biol. Macromol. 84 (2016) 281–288, https://doi.org/10.1016/j.ijbiomac.2015.12.026.

[44] M.A.M. Hussein, M. Grinholc, A.S.A. Dena, I.M. El-Sherbiny, M. Megahed, Boosting the antibacterial activity of chitosan–gold nanoparticles against antibiotic–resistant bacteria by Punicagranatum L. extract, Carbohydr. Polym. 256 (2021), 117498, https://doi.org/10.1016/j.carbpol.2020.117498.
[45] A. Aydogdu, G. Sumnu, S. Sahin, Fabrication of gallic acid loaded hydroxypropyl methylcellulose nanofibers by electrospinning technique as active packaging material, Carbohydr. Polym. 208 (2019) 241–250, https://doi.org/10.1016/j.carbpol.2018.12.065.
[46] R. Kalaivani, M. Maruthupandy, T. Muneeswaran, A. Hameedha Beevi, M. Anand, C.M. Ramakritinan, A.K. Kumaraguru, Synthesis of chitosan mediated silver nanoparticles (Ag NPs) for potential antimicrobial applications, Front. Lab. Med. 2 (2018) 30–35, https://doi.org/10.1016/j.flm.2018.04.002.
[47] M. Valko, C.J. Rhodes, J. Moncol, M. Izakovic, M. Mazur, Free radicals, metals and antioxidants in oxidative stress-induced cancer, Chem. Biol. Interact. 160 (2006) 1–40, https://doi.org/10.1016/j.cbi.2005.12.009.
[48] B. Badhani, N. Sharma, R. Kakkar, ChemInform abstract: gallic acid: a versatile antioxidant with promising therapeutic and industrial applications, RSC Adv. 5 (2015) 27540–27557, https://doi.org/10.1039/C5RA01911G.
[49] M.E. Abd El-Hack, M.T. El-Saadony, M.E. Shafi, N.M. Zabermawi, M. Arif, G. E. Batiha, A.F. Khafaga, Y.M. Abd El-Hakim, A.A. Al-Sagheer, Antimicrobial and antioxidant properties of chitosan and its derivatives and their applications: a review, Int. J. Biol. Macromol. 164 (2020) 2726–2744, https://doi.org/10.1016/j.ijbiomac.2020.08.153.
[50] J. Hernández-Sierra, O. Galicia Cruz, S.-A. Angélica, F. Ruiz, M. Pierdant, A. Pozos-Guillen, In vitro cytotoxicity of silver nanoparticles on human periodontal fibroblasts, J. Clin. Pediatr. Dent. 36 (2011) 37–41, https://doi.org/10.17796/jcpd.36.1.d677647166398886.
[51] A. Galandáková, J. Frankova, N. Ambrožová, K. Habartová, V. Tomšíčková, B. Zalesak, K. Šafářová, M. Smékalová, J. Ulrichová, Effects of silver nanoparticles on human dermal fibroblasts and epidermal keratinocytes, Hum. Exp. Toxicol. 35 (2015), https://doi.org/10.1177/0960327115611969.
[52] P.V. AshaRani, G.L.K. Mun, M.P. Hande, S. Valiyaveettil, Cytotoxicity and genotoxicity of silver nanoparticles in human cells, ACS Nano 3 (2009) 279–290, https://doi.org/10.1021/nn800596w.
[53] A. Roy, O. Bulut, S. Some, A. Mandal, M. Yilmaz, Green synthesis of silver nanoparticles: biomolecule-nanoparticle organizations targeting antimicrobial activity, RSC Adv. 9 (2018) 2673–2702, https://doi.org/10.1039/c8ra08982e.
[54] S. Agnihotri, G. Bajaj, S. Mukherji, S. Mukherji, Arginine-assisted immobilization of silver nanoparticles on ZnO nanorods: an enhanced and reusable antibacterial substrate without human cell cytotoxicity, Nanoscale 7 (2015) 7415–7429, https://doi.org/10.1039/C4NR06913G.
[55] L.K. Vestby, T. Grønseth, R. Simm, L.L. Nesse, Bacterial biofilm and its role in the pathogenesis of disease, Antibiotics 9 (2020) E59, https://doi.org/10.3390/antibiotics9020059 (Basel, Switzerland).